

PRESSURE FLUCTUATION IN HIGH-REYNOLDS NUMBER TURBULENT BOUNDARY LAYER; RESULTS FROM EXPERIMENTS AND NUMERICAL SIMULATIONS

Yoshiyuki Tsuji

Department of Energy Engineering and Science,
Nagoya University
Chikusa-ku, Furo-cho, 464-8603
c42406a@nucc.cc.nagoya-u.ac.jp

Shintaro Imayama

Linné Flow Center,
KTH Mechanics,
SE-100 44 Stockholm, Sweden

Phillipp Schlatter

Linné Flow Center,
KTH Mechanics,
SE-100 44 Stockholm, Sweden

P. Henrik Alfredsson

Linné Flow Center,
KTH Mechanics,
SE-100 44 Stockholm, Sweden

Arne V. Johansson

Linné Flow Center,
KTH Mechanics,
SE-100 44 Stockholm, Sweden

ABSTRACT

Pressure fluctuations are measured in zero-pressure-gradient boundary layers. Following the previous studies, we developed the small pressure probe and measure both the static pressure inside boundary layer and wall pressure simultaneously in turbulent boundary layers up to Reynolds numbers based on the momentum thickness $R_\theta \simeq 20000$. Discussions are made on the background pressure in the free stream region. It contaminates the physical pressure in the boundary layer. We report on the pressure intensity profile normalized by outer and inner variables. Once the background pressure is subtracted, they are compared with the results of direct numerical simulations.

Introduction

The instantaneous pressure fluctuations in the turbulent boundary layer were measured in [1] several years ago. This was the first experimental attempt to discuss the pressure statistics in high Reynolds number boundary layer. The results were reported in TSFP4 and TSFP5. Throughout these researches, we have noticed that the pressure fluctuation inside the boundary layer is affected by free stream condition. In other words, the wall pressure fluctuation has a correlation with static pressure fluctuation even at the point twice the boundary layer thickness. It is significantly different from the trend of velocity statistics.

In the free stream outside boundary layer, there is a potential flow. But the turbulent intensity is not zero exactly in a real wind tunnel, and it is controlled to be as small as possible. The ratio of free stream intensity (u_{rms}/U_0 , here U_0 is free stream velocity and u_{rms} is root mean square of stream-wise velocity fluctuation) should be less than 1 %. It is a criterion how reasonably the turbulent boundary layer develops. On the other hand, about the pressure fluctuation intensity, much at-

tion has not been paid so far. In a real turbulent flow, pressure intensity (expressed as p_{rms} hereafter) is not zero in the free stream. This corresponds to the fact that u_{rms} has some positive value.

In the wind tunnel, there is the inherent signal contamination resulting from facility induced noise. These acoustic disturbances are of low frequency, generally well below 100 Hz. From the Navier-Stokes equation, we obtain the Poisson equation for the instantaneous pressure \tilde{p} . Pressure is calculated by the source term and the boundary conditions. If the acoustic disturbance is contained in the source term, how can we remove this effect and evaluate the physical pressure statistics inside the boundary layer although it may be small. If the boundary condition for the Poisson equation varies depending on the facility, can we expect the universality of pressure statistics inside boundary layer? These are the main concerns in the present study. Recently, new experiments were performed using a smaller pressure sensor in even higher Re number flows. The experimental data are compared with pressure statistics obtained in relatively high Re number direct numerical simulation (DNS) by Schlatter et al.[2] and Jimenez et al.[3]. This may help to answer the above questions.

Experimental Conditions

Pressure fluctuations in the flow field are measured with standard static pressure tube probe (Fig.1). Several calibration techniques have been developed to remove artificial effects such as Helmholtz resonance, standing waves and background noise. The probe body consists of two stainless steel tubes joined by threaded and screwed junctions; the windward tube is cone-shaped and equipped with four static pinholes spaced 90° apart in the circumferential direction and located 12 mm from the tip. This tube has pinhole diameters of $\phi_1 = 0.08\text{mm}$, an inner diameter of 0.3 mm and a

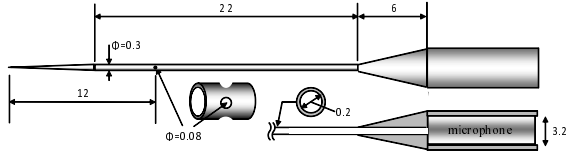


Figure 1. Schematic view of pressure probe.

tube material thickness of $h = 0.05$ mm. The leeward tube begins with a standard 1/8inch condenser microphone with a diameter $d_M = 3.2$ mm. In the previous measurement [1], we were using the probe whose outer diameter is 0.6 mm and $\phi = 0.15$ mm, which were attached to the 1/4 inch microphone. Thus, the present probe size is half approximately. The microphone can perform measurements in the frequency range of $10 - 70 \times 10^3$ Hz, where the lower frequency limit is restricted by its mechanical system. The dynamic range is $2 \times 10^{-2} \sim 3.2 \times 10^3$ Pa, implying that relatively small amplitudes can be measured.

A schematic view of the probe setting in the wind tunnel is shown in Fig.2. Here, a specially designed wall-normal traversing system is used, which protrudes from the plate and allows for traversing in the range $0 \leq y \leq 120$ mm. Another reference probe is set in the free stream, which locates 30 cm from the upper wall surface and measures the pressure fluctuation outside of boundary layer. In the present context, static pressure fluctuation is sometimes referred to simply as pressure fluctuation, and it is expressed as \tilde{p}_s . The pressure fluctuation outside of boundary layer measured by reference probe is expressed as \tilde{p}_b . We call it the back ground pressure fluctuation.

The 1/4 inch microphone is mounted in the cavity volume behind the surface, which is arranged to be as small as possible. The pinhole diameter is $d = 0.3$ mm and its depth is $\ell = 1.0$ mm. Hence the normalized pinhole diameter changes in the range $4.6 \leq d^+ \leq 20.7$ depending on Reynolds number, and the aspect ratio is $\ell/d = 3.33$. From the discussion in [1], the error is estimated to be minimal. In this context, the wall pressure fluctuation is expressed as \tilde{p}_w . Wall pressure and static pressure inside the boundary layer are measured simultaneously and also the pressure in the free stream is monitored. Free stream pressure is used as the reference to remove the background noise generated by the fan and wind tunnel. The experiments were performed in the MTL wind tunnel at KTH. The Reynolds number was varied up to $R_\theta \simeq 21000$. Streamwise velocity is measured by a standard single hot wire, and the wall shear stress is obtained by the oil film interferometry.

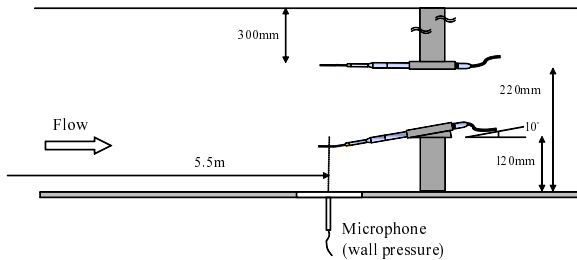


Figure 2. Probe setting in test section.

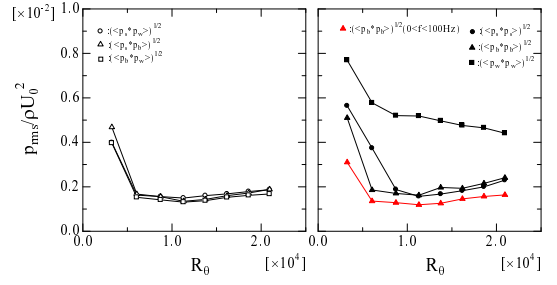


Figure 3. Correlations among p_w , p_s , and p_b . Static probe is set at $y = 120$ mm from the wall.

Results and Discussions

Instantaneous pressure fluctuation measured at the wall, inside boundary layer and free stream, which are expressed as \tilde{p}_w , \tilde{p}_s , \tilde{p}_b , respectively. These pressures are decomposed into their mean and fluctuation as

$$\begin{aligned} \tilde{p}_w &= P_w + p_w, \\ \tilde{p}_s &= P_s + p_s, \\ \tilde{p}_b &= P_b + p_b. \end{aligned} \quad (1)$$

The static pressure probe is set at $y = 120$ mm, where it is about twice boundary layer thickness, and the correlations among p_w , p_s , and p_b are examined. They are normalized by outer variables and are plotted against the Reynolds number in Fig. 3. The correlation $\langle p_s p_b \rangle$ is associated with the fluctuation in the outer region. Because the static pressure probe is set at $y = 120$ mm and the reference probe is $y = 220$ mm. On the other hand, the correlation $\langle p_w p_b \rangle$ represents the large scale fluctuations across the cross section of wind tunnel. These values show almost constant when they are normalized by outer variables, and $\langle p_s p_b \rangle \simeq \langle p_w p_b \rangle$. From these results, we find that the free-stream pressure fluctuation transfers close to the wall immediately. The cross-spectra of p_s and p_w across the boundary layer are plotted in Fig. 4, in which the frequency is multiplied, and usually called the pre-multiplied spectrum (PMS). PMS shapes do not change in the boundary layer, and the contribution comes from the low frequency region $f \leq 100$. The sharp spike around 450 Hz corresponds to the frequency of wind fan. It is convenient to call the free-stream pressure measured by the reference probe the back-ground pressure.

From the results in Fig. 4, we can assume that static pressure inside the boundary layer is contaminated by the back-ground pressure. Then the following decomposition is obtained.

$$\begin{aligned} p_s &= p'_s + p_b, \\ p_w &= p'_w + p_b, \end{aligned} \quad (2)$$

where p'_s and p'_w are static and wall pressure fluctuations besides the back ground pressure. In Fig. 5, we plot the cross

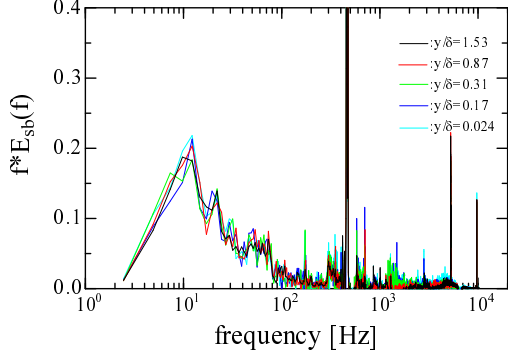


Figure 4. Cross correlation spectra between p_w and p_s . Static pressure position is changed from $y = 0$ mm to $y/\delta = 1.53$ mm.

correlation of p'_s and p'_w and also that of p_s and p_w across the boundary layer, which are normalized by their intensities.

$$\begin{aligned} C(p_s, p_w) &= [E_{p_s p_w}]^2 / [E_{p_s p_s}] [E_{p_w p_w}], \\ C(p'_s, p'_w) &= [E_{p'_s p'_w}]^2 / [E_{p'_s p'_s}] [E_{p'_w p'_w}]. \end{aligned} \quad (3)$$

$$\begin{aligned} \langle p_s p_w \rangle &= \int_0^{+\infty} E_{p_s p_w}(f) df, \\ \langle p_s^2 \rangle &= \int_0^{+\infty} E_{p_s p_s}(f) df, \\ \langle p_w^2 \rangle &= \int_0^{+\infty} E_{p_w p_w}(f) df. \end{aligned} \quad (4)$$

Correlation spectra $C(p_s, p_w)$ show the large value in low frequency region, this is because the contribution from p_b is large. Once the pressure p_b is subtracted, the correlation $C(p'_s, p'_w)$ show the small value in low frequency region, but the correlation is not exactly zero. From the assumption that the background pressure, which is caused by artificial noise, is contaminated in static and wall pressures (Eqs.(3) and (4)) through the boundary layer, we computed the correlation spectra. Static pressure p'_s at the outer edge of boundary layer ($y/\delta \simeq 2\delta$) has still some correlation with wall pressure p'_w . This result shows the difficulty to separate the acoustic noise generated by the flow condition from the physical pressure fluctuations.

In Fig. 6 the root mean square of the pressure fluctuation is plotted versus the distance from the wall in the Reynolds number range $7420 \leq R_\theta \leq 15200$. These data have been corrected by removing the background noise. This is based on the equations (1) and (2), but other corrections are necessary. When they are normalized by inner variables, $p_{rms}^+ \equiv p_{rms} / (\rho u_\tau^2)$, there is a clear R_θ -dependence throughout the boundary layer. The inner rms peak $p_{rms,max}^+$ is according to DNS results located around $y^+ \simeq 30$, and cannot be resolved in these experiments due to physical probe interaction with the wall. With the type of probe used here one cannot

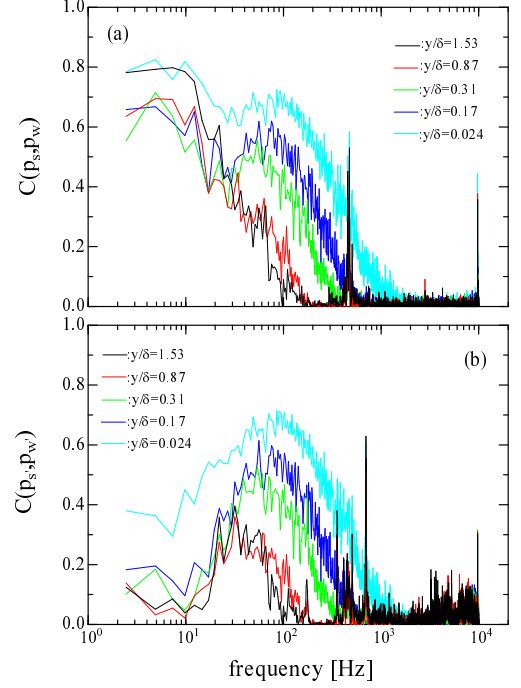


Figure 5. Cross correlation spectra defined by Eq. 3. Static pressure position is changed from $y = 0$ mm to $y = 120$ mm. (a) original signal, (b) back ground pressure is subtracted.

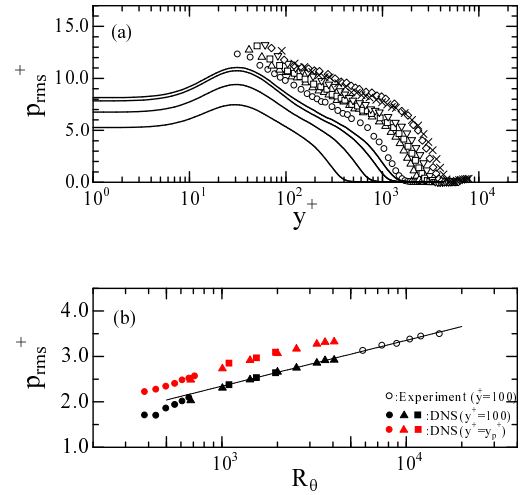


Figure 6. (a) rms of static pressure, normalized using inner variables, are plotted. $\triangle: R_\theta = 7420$, $\square: R_\theta = 8920$, $\nabla: R_\theta = 10500$, $\diamond: R_\theta = 12100$, $\times: R_\theta = 15200$. (b) rms at $y^+ = 100$ with (o)-symbols versus the Reynolds number. Solid symbols indicate the peak of p_{rms}^+ obtained by DNS; \bullet : Skote(2001), \blacksquare : Jimenez(2010), \blacktriangle : Schlatter (2010).

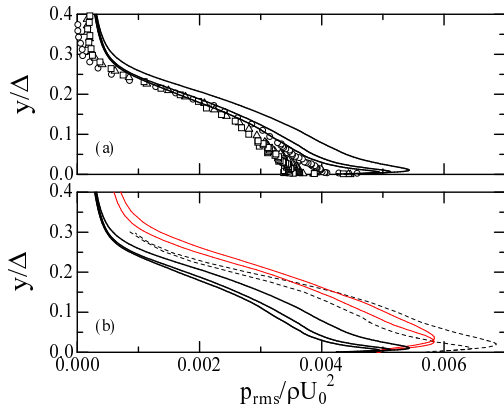


Figure 7. (a) Root mean square of the static pressure, normalized by twice the free stream dynamic pressure. Symbols as in Fig. 7. (b) Similar distributions obtained with DNS. Solid lines are by Skote(2001) at $R_\theta = 450, 716$, and dashed lines are by Spalart(1988) at $R_\theta = 670, 1410$, Schlatter (2010) at $R_\theta = 2000, 3270, 4060$.

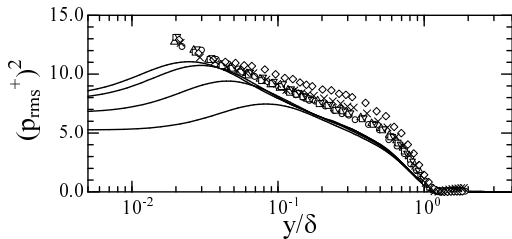


Figure 8. rms of static pressure, normalized using inner and outer variables, are plotted. Symbols are the same with those in Fig. 6. Solid lines are DNS by Schlatter (2010) at $R_\theta = 1000, 2000, 3270, 4060$.

get closer to the wall than $y^+ \approx 40$ and 90 for $R_\theta = 7420$ and 15200 , respectively.

Direct numerical simulations show that the maximum value $p_{rms,max}^+$ increases as the Reynolds number increases. This Reynolds number dependence is shown in Fig. 7. The distributions are well approximated by a logarithmic function ; $p_{rms,max}^+ \propto \ln(R_\theta)$. The experimental data, as plotted with (\circ)-symbols in figure, are the pressure r.m.s. at $y^+ = 100$. DNS and experimental data show the similar Reynolds num-

ber dependence.

On the other hand, when the pressure rms is normalized by outer variables, ρU_0^2 , and the distance from the wall with Δ , the profiles more or less collapse on each other in the outer region as shown in Fig. 7(a). Here Δ is Rotta-Clauser boundary layer thickness, and U_0 is free-stream velocity. Figure 7(b) shows the DNS results by Skote (2001), Spalart (1988), Philipp et al (2010) in comparison with experiment. We can recognize a Reynolds number dependence when R_θ is small. The peak $p_{rms,max}^+ / \rho U_0^2$ increases, and moves closer to the wall in terms of y/Δ as the Reynolds number increases.

Figure 8 shows the normalization by outer length and inner velocity scales. As Reynolds number increases, larger peak values closer to the wall are observed. And there is overlap region where the relation $(p_{rms}^+)^2 \propto \ln(y/\delta)$. In the experimental data, the profile is slightly different from that of DNS. This may be because the background pressure, artificial effect, is not perfectly removed from the physical pressure fluctuation in the present techniques.

About the wall pressure rms, we studied the Reynolds number dependence when it is normalized with inner, outer and mixed scaling. For the inner scaling, wall pressure rms, $p_{w,rms}^+$, increases slowly with increasing Reynolds number. The profiles are wall approximated by the relation of $(p_{w,rms}^+)^2 \propto \ln(R_\theta)$. The behaviour of p_{rms} normalized by outer variables seen to decrease as the Reynolds number increases but appears to reach an asymptotic value for high R_θ . However, it is seen that by normalizing the pressure with mixed scaling, we obtain an overall small variation of the normalized rms-level, but for high R_θ , it tends to increase slightly. These trends are well observed in the results of Direct numerical simulations. The details are reported in the presentation.

REFERENCES

- [1]Y. Tsuji, J. Fransson, H. Alfredsson, and A. V. Johansson, "Pressure Statistics and Their Scaling in High-Reynolds-number Turbulent Boundary Layers", J.Fluid Mech., Vol.585,pp.1-40(2007).
- [2] P. Schlatter and R. Orlu, J. Fluid Mech., "Assessment of Direct Numerical Simulation Data of Turbulent Boundary Layers", Vol. 659, pp. 116-126(2010).
- [3]J. Jimenez, S. Hoyas, M. P. Simens, Y. Mizuno, "Turbulent boundary layers and channels at moderate Reynolds numbers", J.Fluid Mech.,Vol. 657, pp. 335-360 (2010).
- [4]M. Skote, "Studies of Turbulent Boundary Layer Flow through Direct Numerical Simulation", TRITA-MEK Tech. Rep. 2001:01, Dept. Mech., KTH, Stockholm, Sweden, (2001)